Journal of Cerebral Blood Flow & Metabolism (2012) 32, 1073–1085

www.jcbfm.com

Use of spectral analysis with iterative filter for voxelwise determination of regional rates of cerebral protein synthesis with L-[1-^{11}C]leucine PET

Mattia Veronese[1], Kathleen C Schmidt[2], Carolyn Beebe Smith[2] and Alessandra Bertoldo[1]

[1]*Department of Information Engineering, University of Padova, Padova, Italy;* [2]*Section of Neuroadaptation and Protein Metabolism, National Institute of Mental Health, Bethesda, Maryland, USA*

A spectral analysis approach was used to estimate kinetic parameters of the L-[1-^{11}C]leucine positron emission tomography (PET) method and regional rates of cerebral protein synthesis (*rCPS*) on a voxel-by-voxel basis. Spectral analysis applies to both heterogeneous and homogeneous tissues; it does not require prior assumptions concerning number of tissue compartments. Parameters estimated with spectral analysis can be strongly affected by noise, but numerical filters improve estimation performance. Spectral analysis with iterative filter (SAIF) was originally developed to improve estimation of leucine kinetic parameters and *rCPS* in region-of-interest (ROI) data analyses. In the present study, we optimized SAIF for application at the voxel level. In measured L-[1-^{11}C]leucine PET data, voxel-level SAIF parameter estimates averaged over all voxels within a ROI (mean voxel-SAIF) generally agreed well with corresponding estimates derived by applying the originally developed SAIF to ROI time-activity curves (ROI-SAIF). Region-of-interest-SAIF and mean voxel-SAIF estimates of *rCPS* were highly correlated. Simulations showed that mean voxel-SAIF *rCPS* estimates were less biased and less variable than ROI-SAIF estimates in the whole brain and cortex; biases were similar in white matter. We conclude that estimation of *rCPS* with SAIF is improved when the method is applied at voxel level than in ROI analysis.
Journal of Cerebral Blood Flow & Metabolism (2012) **32,** 1073–1085; doi:10.1038/jcbfm.2012.27; published online 7 March 2012

Keywords: [^{11}C]leucine; cerebral protein synthesis; parametric imaging; positron emission tomography; spectral analysis

Introduction

Functional quantification with positron emission tomography (PET) is generally based on kinetic modeling approaches that relate a particular biological process of interest to measurements of activity in blood and tissue following administration of a radiolabeled tracer. Kinetic models used in PET are necessarily simplified representations of tissue processes, and one of the simplifying assumptions frequently made is that tissue regions are kinetically homogeneous, that is, rates of blood flow, delivery and efflux of tracer to/from tissue, metabolism, and incorporation into labeled products do not vary in the tissue region. In the brain, these assumptions are difficult to meet. At spatial resolutions approximately an order of magnitude higher than PET, such as achieved in autoradiographic studies, one clearly sees heterogeneity of rates of blood flow, glucose metabolism, and protein synthesis across the brain (Schmidt and Smith, 2005). Not only are rates of these processes different in gray and white matter, but within gray matter structures themselves, for example in cortical layers, rates of these processes can vary considerably. At the relatively lower spatial resolution of PET scanning, therefore, activities measured in the brain can be expected to originate from kinetically heterogeneous mixtures of tissue. Application of kinetic models designed for homogeneous tissues to heterogeous tissues leads to errors in estimated rates of cerebral blood flow and glucose metabolism, as well as to errors in estimates of receptor binding parameters (Schmidt and Turkheimer, 2002).

Correspondence: Dr A Bertoldo, Department of Information Engineering (DEI), University of Padova, Via G Gradenigo 6/B, 35131 Padova, Italy.
E-mail: bertoldo@dei.unipd.it
This research was supported in part by the Intramural Research Program, National Institute of Mental Health. Portions of this work were presented in preliminary form at The Eighth International Symposium on Functional Neuroreceptor Mapping of the Living Brain (NRM2010) (Veronese *et al*, 2010*b*).
Received 14 October 2011; revised 20 January 2012; accepted 6 February 2012; published online 7 March 2012

Protein synthesis in the nervous system is a fundamental process essential for adaptive responses such as long-term memory formation. With L-[1-^{11}C]leucine and PET, it is possible to fully quantify the measurements of regional rate of cerebral protein synthesis (*rCPS*) in human subjects (Schmidt *et al*, 2005; Smith *et al*, 2005). Quantification of *rCPS* with the L-[1-^{11}C]leucine PET method was initially carried out at the region-of-interest (ROI) level and was based on a kinetic model that assumes tissue ROIs are kinetically homogeneous (Schmidt *et al*, 2005); effects of tissue heterogeneity were not taken into account.

We recently reported two approaches to address effects of tissue heterogeneity on *rCPS* estimated in [^{11}C]leucine PET studies: reducing the size of tissue regions by using a voxel-by-voxel analysis, while retaining the tissue homogeneity assumption (Tomasi *et al*, 2009) and, conversely, by keeping data analysis at the ROI level, but employing a spectral analytic approach that applies to heterogeneous as well as homogeneous tissues (Veronese *et al*, 2010*a*). Use of the voxelwise analysis reduced, but did not entirely eliminate, effects of tissue heterogeneity visible in model fits of measured tissue time-activity curves (*TACs*) (Tomasi *et al*, 2009). The spectral analytic approach, spectral analysis with iterative filter (SAIF), detected heterogeneity in all ROIs examined (Veronese *et al*, 2010*a*). Not all parameters are identifiable in heterogeneous tissue, however, without use of parameter constraints. Specifically, determination of *rCPS* requires an estimate of the fraction of unlabeled leucine in the precursor pool for protein synthesis that is derived from arterial plasma. This quantity is defined as λ. In a homogeneous tissue, λ can be calculated directly from kinetic model or SAIF parameters, whereas in a heterogeneous tissue values of λ in different tissue subregions are not individually identifiable. As a first approximation, we introduced the constraint that values of λ in all tissue subregions are equal, and on that basis λ and *rCPS* in heterogeneous tissue were estimated. Under this constraint, differences between *rCPS* estimated with SAIF at the ROI level and *rCPS* estimated by homogenous voxelwise analysis were small (mean relative difference $\sim$2%), but *rCPS* determined with SAIF had a tendency to be somewhat lower in the whole brain and cortical regions, and higher in some subcortical and white matter regions, than *rCPS* determined by voxelwise analysis (Veronese *et al*, 2010*a*). The equality constraint on λ was understood to be an imperfect approximation, as parametric maps of λ show some spatial variation (Tomasi *et al*, 2009), but sensitivity analysis suggested that the use of the constraint should have only a small effect on calculated *rCPS* (Veronese *et al*, 2010*a*).

In the current study, we investigated the possibility of adapting SAIF to estimate parameters of the [^{11}C]leucine kinetic model on a voxel-by-voxel basis. Our aim was to develop a method to deal with heterogeneity at the voxel level, the degree of which may be dependent on the resolution of the PET scanner. Reducing the size of the tissue volume examined may also reduce effects arising from the equality constraint on the λs in all subregions of heterogeneous tissues. Due to vastly different signal-to-noise ratios in voxel and ROI data, SAIF developed for ROI analysis could not be directly used for voxelwise estimation. In the present study, the SAIF method was optimized for high levels of noise typical of voxelwise data, and simulations were performed to assess precision and accuracy of parameter estimates. We also investigated the capacity of SAIF to correctly identify the number of kinetic components in each voxel. The method was then used to reanalyze data from previously acquired L-[1-^{11}C]leucine PET studies in six awake healthy young men.

Materials and methods

Spectral Analysis Iterative Filter

The spectral analysis method is based on a single input–single output model used to identify kinetic components of tissue tracer activity (Cunningham and Jones, 1993; Turkheimer *et al*, 1994). The system output, concentration of radioactivity in tissue, $C^*_{\mathrm{tiss}}(t)$, is described by the convolution of the input function, that is, plasma concentration of parent tracer, $C^*_{\mathrm{p}}(t)$, with an exponential transfer function that has real-valued, nonpositive exponents. That is,

$$C^*_{\mathrm{tiss}}(t) = \sum_{j=0}^{M} C^*_{\mathrm{p}}(t) \otimes \alpha_j \mathrm{e}^{-\beta_j t} = \sum_{j=0}^{M} \alpha_j \int_0^t C^*_{\mathrm{p}}(\tau)\mathrm{e}^{-\beta_j(t-\tau)}\mathrm{d}\tau \quad (1)$$

where α_j and β_j are assumed to be real-valued and nonnegative. Not all compartmental models satisfy these assumptions, but they are met by the kinetic models used with many PET tracers (Schmidt, 1999) including L-[1-^{11}C]leucine (Veronese *et al*, 2010*a*). In spectral analysis, the maximum number of terms to be included in the model and the possible values of β_j are preset, and the α_j are estimated from measured blood and tissue *TACs* (Cunningham and Jones, 1993). The estimated spectrum of kinetic components, together with knowledge of the tracer's biochemical and/or physiological properties, is then related to the process of interest. The number of compartments in the kinetic model of the tracer is also obtained (Bertoldo *et al*, 1998).

From equation (1) one observes that 'high-frequency' components (β_j very large) equilibrate rapidly with and become proportional to $C^*_{\mathrm{p}}(t)$, whereas 'low-frequency' components ($\beta_j \cong 0$) are proportional to $\int C^*_{\mathrm{p}}(t)\mathrm{d}t$ and account for trapping of tracer. Components with intermediate values of β_j reflect tissue compartments that exchange material directly or indirectly with plasma; these are referred to as equilibrating components. Noise in the data greatly influences the accuracy with which very

low- and high-frequency components can be detected, and the problem is exacerbated when the method is applied where the signal-to-noise ratio is low. In these cases, application of numerical filters becomes essential. Spectral analysis iterative filter, previously developed for estimating *rCPS* from region-of-interest data (Veronese *et al*, 2010*a*), was investigated in the present study for use with voxelwise estimation. Spectral analysis with iterative filter uses a passband filter $[\beta_L,\beta_U]$ to separate trapping and blood components from equilibrating components. The passband lower limit β_L represents the smallest exponent β for a component that can be distinguished from trapping of tracer, and the upper limit β_U is the largest exponent of a component that can be distinguished from blood in the brain. The passband limits are determined based on prior information on expected tracer kinetics, data sampling schedule, and noise in the data. As in the previous study, we utilized 100 logarithmically distributed values β_j between 0.0038 and 1.3 min^{-1} in the estimations (Veronese *et al*, 2010*a*). Spectral analysis with iterative filter conserves the main characteristics of spectral analysis—it does not require any prior assumptions concerning number of compartments in the system, and it can be applied to heterogeneous as well as homogeneous tissues. The added benefit of SAIF is that it improves estimates of both α_0 and $\sum_{i=1}^{n}\alpha_i$ whose accurate estimation is essential for quantification of *rCPS* (Veronese *et al*, 2010*a*).

Leucine Kinetic Model

The model for L-[1-^{11}C]leucine that explicitly allows for tissue heterogeneity is shown in Figure 1A. The model assumes that each tissue is composed of n subregions ($n \geqslant 1$), and the kinetics of L-[1-^{11}C]leucine in each subregion are described by the homogeneous tissue model given in Schmidt *et al* (2005). Activity in the tissue as a whole is a convex combination of activity in its subregions. The model used to describe labeled leucine holds also for unlabeled leucine (Figure 1B), except that unlabeled leucine and protein are in steady state. Assuming no isotope effect, rate constants for unlabeled and labeled leucine are identical. The steady-state breakdown of unlabeled protein is greater than zero.

When total activity in a brain region or voxel following injection of L-[1-^{11}C]leucine is written in terms of the spectral analysis parameters (symbols are defined as follows: C_T*, total ^{11}C concentration in volume (region or voxel); V_b, fraction of volume occupied by blood; C_p*, concentration of L-[1-^{11}C]leucine in arterial plasma; C_b*, total ^{11}C concentration in whole blood; V_D, brain:blood equilibrium distribution volume of $^{11}CO_2$ (fixed at 0.41); C_c*, $^{11}CO_2$ concentration in whole blood; K_{1i} rate constant in i^{th} subregion for transport of leucine from plasma to tissue; k_{2i}, rate constant in i^{th} subregion for transport of leucine from tissue to plasma; k_{3i}, rate constant in i^{th} subregion for the first two steps in leucine catabolism, transamination, and decarboxylation, which yield $^{11}CO_2$; k_{4i}, rate constant in i^{th} subregion for leucine incorporation into protein; w_i, relative tissue weight of i^{th} subregion; n, number of homogeneous tissue subregions), we obtain (Veronese *et al*, 2010*a*)

$$C_T^*(t) = (1-V_b)\cdot\left\{\alpha_0\cdot\int_0^t C_p^*(\tau)d\tau\ldots + \alpha_a\cdot\int_o^t C_p^*(\tau)e^{-\beta_a(t-\tau)}d\tau + \alpha_b\cdot\int_o^t C_p^*(\tau)e^{-\beta_b(t-\tau)}d\tau + \ldots + \alpha_n\cdot\int_o^t C_p^*(\tau)e^{-\beta_n(t-\tau)}d\tau + V_D C_c(t)\right\} + V_b C_b(t) \quad (2)$$

where

$$\beta_i = k_{2i} + k_{3i} + k_{4i} \quad (3)$$

$$\alpha_0 = \sum_{i=a}^{n}\frac{w_i K_{1i} k_{4i}}{k_{2i}+k_{3i}+k_{4i}} \quad (4)$$

$$\alpha_i = \frac{w_i K_{1i}(k_{2i}+k_{3i})}{k_{2i}+k_{3i}+k_{4i}} \quad i = a, b, \ldots, n. \quad (5)$$

Spectral analysis with iterative filter is used to estimate n and the spectral analysis parameters α_0, α_a, α_b, …, α_n, β_a, β_b, …, β_n, and V_b. From these parameters, the leucine parameters of interest can be determined. The latter include the weighted average influx rate constant for the mixed tissue, $K_1 \equiv \sum_{i=1}^{n} w_i K_{1i}$, which can be estimated as

$$K_1 = \alpha_0 + \sum_{i=1}^{n}\alpha_i. \quad (6)$$

The fraction of unlabeled leucine in the precursor pool for protein synthesis in tissue subregion i that is derived from arterial plasma, $\lambda_i \equiv (k_{2i}+k_{3i})/(k_{2i}+k_{3i}+k_{4i})$ is identified for each subregion under the constraint that $\lambda_a = \lambda_b = \ldots = \lambda_n = \lambda$, as

$$\lambda = \frac{K_1 - \alpha_0}{K_1}. \quad (7)$$

Finally, *rCPS* in the mixed tissue can be computed as

$$rCPS = \frac{\alpha_0}{\lambda}C_p, \quad (8)$$

where C_p is the arterial plasma concentration of unlabeled leucine.

Simulation Studies

Simulation 1: Spectral analysis with iterative filter passband: Due to the large discrepancy in signal-to-noise ratio between voxel and ROI *TACs*, the equilibrating component passband optimized for ROI analysis may not be optimal for voxelwise quantification. To define the passband interval bounds $[\beta_L,\beta_U]$, we followed a simulation strategy similar to that used for application of SAIF at the ROI level (Veronese *et al*, 2010*a*). The procedure consisted of simulating noisy voxel-*TACs* that were subsequently

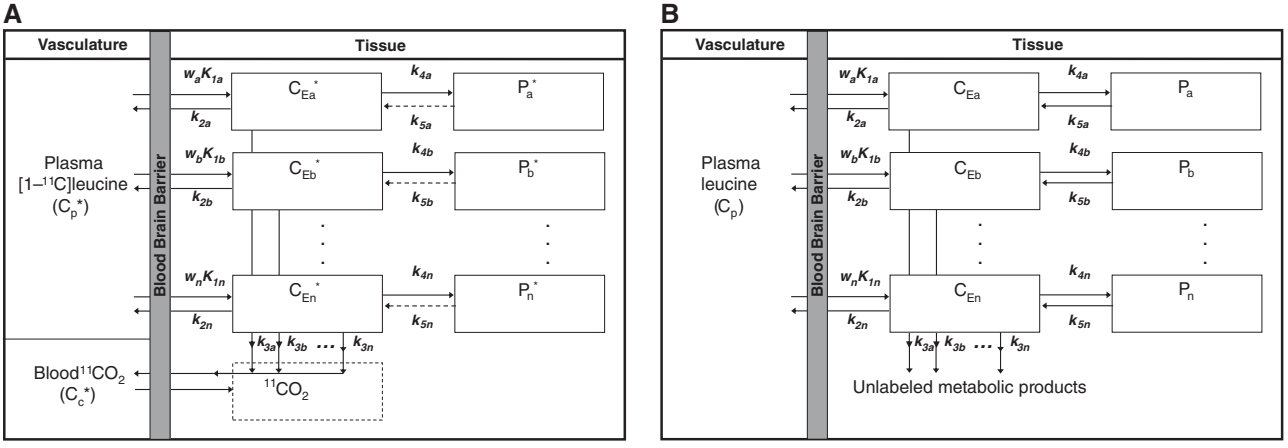

Figure 1 (**A**) Heterogeneous tissue model for L-[1-^{11}C]leucine. The heterogeneous tissue is composed of n kinetically homogeneous subregions. The constants w_a, w_b, …, w_n represent relative tissue weights of the subregions, where $w_a + w_b + \ldots + w_n = 1$. In each subregion i, K_{1i} and k_{2i} are the rate constants for transport of leucine from plasma to tissue and back, respectively. k_{3i} is the rate constant for the first two steps in leucine catabolism, transamination, and decarboxylation, which yield $^{11}CO_2$. k_{4i} and k_{5i} are the rate constants for leucine incorporation into protein and for the release of free leucine from proteolysis, respectively. Because of the long half-life of protein in the brain (Lajtha *et al*, 1976), it is assumed that there is no significant breakdown of labeled product (P_i*) during the experimental interval, that is, $k_{5i}P_i^* \sim 0$. Under the assumptions of negligible fixation of $^{11}CO_2$ during the experimental period (Siesjo and Thompson, 1965) and rapid equilibration of $^{11}CO_2$ between the brain and blood (Buxton *et al*, 1987), the model for each subregion reduces to two-tissue compartments (free L-[1-^{11}C]leucine, C_{Ei}*, and L-[1-^{11}C]leucine incorporated into tissue protein, P_i*) plus the $^{11}CO_2$ compartment in which the concentration is assumed known. In each subregion, the kinetics of leucine are described by the homogeneous tissue model given in Schmidt *et al* (2005), which assumes that the concentrations of amino acids, rates of blood flow, rates of transport and metabolism of amino acids, and rates of leucine incorporation into protein do not vary within the subregion. Total tracer activity ($C_T^*(t)$) in the volume is given by

$$\begin{aligned} C_{\mathrm{T}}^*(t) =& (1-V_{\mathrm{b}})\left\{\left(\frac{w_aK_{1a}(k_{2a}+k_{3a})}{k_{2a}+k_{3a}+k_{4a}}\right)\int_0^t C_{\mathrm{p}}^*(\tau)\mathrm{e}^{-(k_{2a}+k_{3a}+k_{4a})(t-\tau)}\mathrm{d}\tau\right. \\ &+\left(\frac{w_bK_{1b}(k_{2b}+k_{3b})}{k_{2b}+k_{3b}+k_{4b}}\right)\int_0^t C_{\mathrm{p}}^*(\tau)\mathrm{e}^{-(k_{2b}+k_{3b}+k_{4b})(t-\tau)}\mathrm{d}\tau+\ldots \\ &+\left(\frac{w_nK_{1n}(k_{2n}+k_{3n})}{k_{2n}+k_{3n}+k_{4n}}\right)\int_0^t C_{\mathrm{p}}^*(\tau)\mathrm{e}^{-(k_{2n}+k_{3n}+k_{4n})(t-\tau)}\mathrm{d}\tau \\ &+\left(\frac{w_aK_{1a}k_{4a}}{k_{2a}+k_{3a}+k_{4a}}+\frac{w_bK_{1b}k_{4b}}{k_{2b}+k_{3b}+k_{4b}}+\ldots+\frac{w_nK_{1n}k_{4n}}{k_{2n}+k_{3n}+k_{4n}}\right)\int_o^t C_{\mathrm{p}}^*(\tau)\mathrm{d}\tau \\ &\left.+V_{\mathrm{D}}C_{\mathrm{C}}^*(t)\right\}+V_{\mathrm{b}}C_{\mathrm{b}}^*(t), \end{aligned}$$

where V_b is the fraction of the volume occupied by blood; C_b^* is the total ^{11}C concentration in whole blood; V_D is the brain:blood equilibrium distribution volume of $^{11}CO_2$; and C_c^* is the $^{11}CO_2$ concentration in whole blood. V_D is fixed at 0.41 (Smith *et al*, 2005; Brooks *et al*, 1984). (**B**) Heterogeneous tissue model for unlabeled leucine. The model used to describe labeled leucine (**A**) also holds for unlabeled leucine. Assuming no isotope effect, rate constants for labeled and unlabeled leucine are identical. The model for unlabeled leucine in heterogeneous tissue is composed of n homogeneous subregions; in each homogeneous tissue the unlabeled leucine (C_{Ei}) and protein (P_i) are assumed to be in steady state, and the steady-state breakdown unlabeled protein ($k_{5i}P_i$) is greater than zero. Therefore, the weighted average of regional rate of cerebral protein synthesis (*rCPS*) is

$$rCPS = \left(\frac{w_aK_{1a}k_{4a}}{k_{2a}+k_{3a}}+\frac{w_bK_{1b}k_{4b}}{k_{2b}+k_{3b}}+\ldots+\frac{w_nK_{1n}k_{4n}}{k_{2n}+k_{3n}}\right)C_{\mathrm{p}},$$

where C_p is the concentration of unlabeled leucine in arterial plasma and the rate constants are defined above (Schmidt *et al*, 2005; Veronese *et al*, 2010*a*). The fraction of unlabeled leucine in the precursor pool for protein synthesis in subregion i that is derived from arterial plasma, λ_i, can be expressed as

$$\lambda_i = \frac{k_{2i}+k_{3i}}{k_{2i}+k_{3i}+k_{4i}} \text{ for } i = a, b, \ldots, n.$$

and the weighted average influx rate constant for the mixed tissue, K_1, as

$$K_1 = w_aK_{1a} + w_bK_{1b} + \cdots + w_nK_{1n}.$$

analyzed by SAIF with different passband intervals. The optimal passband was chosen as the one that provided the best trade-off between precision and accuracy of the estimates of *rCPS* and other parameters of interest.

Noise-free voxel-*TACs* were simulated according to a heterogeneous kinetic model, with two equilibrating components and one trapping component. Model parameters were generated by the random sampling of normal distributions as follow: $V_b = 0.064 \pm 0.009$ (unitless), $\alpha_0 = 0.012 \pm 0.002$ ($mL\,g^{-1}\,min^{-1}$), $\alpha_1 = 0.0096 \pm 0.0004$ ($mL\,g^{-1}\,min^{-1}$), $\alpha_2 = 0.0197 \pm 0.0015$ ($mL\,g^{-1}\,min^{-1}$), $\beta_0 = 0$ (min^{-1}), $\beta_1 = 0.032 \pm 0.004$ (min^{-1}), and $\beta_2 = 0.15 \pm 0.03$ (min^{-1}). These values are the intersubject mean values ± s.d. of spectra estimated with ROI-SAIF in whole brain (Veronese *et al*, 2010*a*). One thousand noisy *TACs* were simulated by adding to the noise-free simulated *TACs* Gaussian noise with zero-mean and variance consistent with the level of noise in voxel data, as estimated in Tomasi *et al* (2009). Different passband intervals ($\beta_L = 0.005$ to $0.06\ min^{-1}$; $\beta_U = 0.1$ to $0.6\ min^{-1}$) were tested. To select the best interval, performance indices percent bias (*Bias%*) and percent root mean square error (*RMSE%*) were computed as

$$Bias\% = 100 \cdot \left[\frac{1}{K}\sum_{r=1}^{K} bias_r\right] = 100 \cdot \left[\frac{1}{K}\sum_{r=1}^{K}\frac{(p_r - p_{TRUE,r})}{p_{TRUE,r}}\right] \quad (9)$$

and

$$RMSE\% = 100 \cdot \sqrt{\sum_{r=1}^{K}\frac{\left(bias_r - \frac{1}{K}\cdot\sum_{s=1}^{K} bias_s\right)^2}{K}} \quad (10)$$

where p_r represents the r^{th} SAIF parameter estimate, $p_{TRUE,r}$ indicates the true parameter value for the r^{th} simulated *TAC*, $bias_r$ indicates bias for the r^{th} simulated *TAC*, and K indicates total number of simulated *TACs*. Any noise realization that resulted in a negative entry in the simulated *TAC* was discarded and replaced with a new realization.

Simulation 2: performance of voxelwise spectral analysis with iterative filter: Once the choice of passband was made, a new simulation was performed to quantify the effect of noise on estimated parameters of interest. In these simulations, a bootstrap approach was used as an alternative to random noise generation with a Gaussian model.

To simulate data as close as possible to that measured in a previously acquired PET study, we proceeded as follows:

(1) Using the optimal passband interval obtained in Simulation 1, data measured in a representative slice of an individual brain volume, masked to include brain voxels only, were analyzed voxel-by-voxel with SAIF. The set of parameters obtained became the reference, or 'true,' parameter values used in the simulations. Outliers and algorithm failures produced at this step were excluded from the simulation.
(2) Noise-free *TACs* were generated by convolving the original measured arterial input function of the subject with the sum of exponential terms defined by the reference parameters from step 1. In addition, for each voxel, normalized residuals $R_i(t)$ were computed as:

$$R_i(t) = \frac{C^*_{T,i}(t) - TAC_i(t)}{\max\left[C^*_{T,i}(t)\right]} \quad i = 1, 2, \ldots, K \quad (11)$$

where $C^*_{T,i}(t)$ represents total concentration of ^{11}C in the field of view of the PET camera for the i^{th} voxel, $TAC_i(t)$ indicates the noise-free *TAC* for the i^{th} voxel, and K is the number of voxels in the chosen slice.
(3) Voxel noise was simulated using a bootstrap approach (Efron, 1979) based on random resampling of normalized residuals. With this approach, noise for the i-th voxel ($N_i(t)$) was simulated as

$$N_i(t) = R_j(t) \cdot \max[TAC_i(t)] \quad i = 1, 2, \ldots, K;\ j \in \{1, 2, \ldots, K\} \quad (12)$$

where $R_j(t)$ is the resampled normalized residual, originally associated with the j^{th} voxel, chosen by random sampling with replacement from among all brain voxels of the slice.
(4) Noisy voxel-*TACs* were generated by adding the simulated noise to the noise-free *TACs* as

$$TAC_i(t)\text{noisy} = TAC_i(t) + N_i(t) \quad i = 1, 2, \ldots, K \quad (13)$$

The procedure was repeated 50 times, generating 50 different bootstrap-simulated slices. Note that the bootstrap procedure used here differs from the usual approach of normalizing each residual vector by its standard deviation in order to assure that all resampled residuals have equal variance. In this approach, the required rescaling would be by the standard deviation in the target voxel residual. In the current study, however, we do not have good estimates of the variance in each individual voxel due to the inherent high noise levels of voxel data. Instead, we empirically chose normalization and rescaling to the maxima of the *TACs*, as these scale factors have the added advantage of preventing negative values in the simulated noisy *TACs*. The sample variances of the original and bootstrapped residuals were compared to check the effect of the chosen scale factors.

All 50 bootstrap-simulated slices were analyzed with the voxelwise SAIF approach. Spectral analysis with iterative filter applied at the voxel level with the passband interval optimized for voxel analyses will be referred to as voxel-SAIF. We looked at three regions: the whole slice and two ROIs placed on the slice (frontal cortex and corona radiata). As in Simulation 1, to assess the quality of voxel-SAIF results, for each region and each parameter of interest, *Bias%* and *RMSE%* were computed. The number of voxels with estimated parameter values considered to be outside the normal physiological range, that is, those with

$K_1 > 1\,\text{mL}\,\text{g}^{-1}\,\text{min}^{-1}$, $V_b > 1$, or $rCPS > 10\,\text{nmol}\,\text{g}^{-1}\,\text{min}^{-1}$, was recorded (all SAIF parameter estimates are already restricted to be nonnegative by algorithm design), and outlier voxels were excluded from *bias* and *RMSE* statistics. For comparison, we also averaged voxel-*TACs* in each bootstrap-simulated slice over the three regions to obtain ROI *TACs*, which were then analyzed with SAIF using the passband interval optimized for ROI data (ROI-SAIF) (Veronese *et al*, 2010*a*).

We also investigated the capacity of voxel-SAIF to correctly identify the number of kinetic components in each voxel by comparing the number of tissue equilibrating components in the reference data with the number detected in bootstrap-simulated slices.

Positron Emission Tomography Studies

Data from previously reported studies (Bishu *et al*, 2008, 2009) of six healthy awake male subjects were reanalyzed in the current study. Subject inclusion criteria and the PET study procedure are described in detail in Bishu *et al* (2008). Briefly, all subjects underwent 90-minute dynamic L-[1-^{11}C]leucine scan on a ECAT High-Resolution Research Tomograph, with a spatial resolution of ~ 2.6 mm full width at half maximum (Wienhard *et al*, 2002). Images were reconstructed and motion-corrected (Carson *et al*, 2003) as 42 frames of data (16×15, 4×30, 4×60, 4×150, 14×300 seconds); voxel size was $1.21 \times 1.21 \times 1.23\,\text{mm}^3$. Arterial blood was sampled over the course of the study and concentrations of unlabeled and labeled leucine in arterial plasma and total ^{11}C and $^{11}CO_2$ activities in whole blood were measured (Bishu *et al*, 2008). All subjects underwent a T1-weighted brain MRI (magnetic resonance imaging) for the ROI placement. The MRI was registered to the mean of the 30 to 60 minutes PET leucine data, and ROI masks were resliced on PET space (Tomasi *et al*, 2009).

The whole brain and 12 regions were evaluated in all subjects. Estimates of V_b, K_1, λ, and *rCPS* were determined in each ROI and in each voxel by using ROI-SAIF and voxel-SAIF, respectively. Weights were inversely proportional to the variance of decay-corrected measured activity in the region, which was modeled assuming Poisson statistics as

$$\text{var}(C_T^*(t_i)) = \rho \frac{e^{\gamma t_i} C_T^*(t_i)}{\Delta t_i} \qquad (14)$$

(Wu and Carson, 2002), where γ is the decay constant for ^{11}C, Δt_i is length of Frame i, and ρ is a proportionality coefficient reflecting the noise level in the data estimated *a posteriori* (Veronese *et al*, 2010*a*). For voxel-SAIF, weights were based on whole brain activity; in ROI-SAIF, weights were based on activity in the region itself. Tracer arrival delay was calculated as in Veronese *et al* (2010*a*).

For all subjects, ROI-SAIF estimates were compared with the mean of voxel-SAIF estimates in all voxels of the region. To assess agreement between methods, we calculated the slope and intercept of the fitted regression line with ROI-SAIF estimates and mean voxel-SAIF estimates in each region and each subject as independent and dependent variables, respectively. Pearson's R^2 values were added as correlation measures.

We also visually examined the spatial distribution of voxels found to be kinetically heterogeneous. The 'heterogeneity map' was constructed by fusing the MR image with a map of the spatial distribution of voxels with two or more SAIF-estimated equilibrating components.

Results

Simulation 1: Spectral Analysis with Iterative Filter Passband

In simulations performed to find an appropriate filter passband, *rCPS bias* ranged from 3% to 25%, depending on the cutoff frequencies β_L and β_U. Root mean square error ranged from 15% to 35% for *rCPS* estimates, and from 8% to 38% for the other parameters of interest, that is, K_1, λ, and V_b. Due to the high level of noise typical of voxel-*TACs*, these values were much higher than those obtained with ROI-SAIF (*bias* in *rCPS*: 0.03% to 7%; *RMSE* 2.4% to 21.5% (Veronese *et al*, 2010*a*)). For voxel-SAIF, we chose 0.02 min^{-1} and 0.2 min^{-1} for β_L and β_U, respectively, as a good compromise between precision and accuracy of *rCPS* (*bias* 3%; *RMSE* 18%) and λ (*bias* 2%; *RMSE* 8%). With this passband interval, K_1 and V_b displayed, respectively, 8% and 6% *bias*, and 14% and 28% *RMSE*. This choice for the voxel-SAIF passband interval differs from that made for ROI-SAIF ($\beta_L = 0.03$ min^{-1}; $\beta_U = 0.3$ min^{-1}) (Veronese *et al*, 2010*a*); when the optimal ROI passband was applied to voxelwise analysis bias exceeded 5% for all parameters of interest.

In the following text, voxel-SAIF refers to SAIF applied at voxel level with its optimal passband of [0.02, 0.2] min^{-1}, and ROI-SAIF refers to SAIF applied at the ROI level with its optimal passband interval of [0.03, 0.3] min^{-1}.

Simulation 2: Performance of Voxel-Spectral Analysis with Iterative Filter

Less than 1% of brain voxels in the slice were excluded from the bootstrap simulations due to outlier parameter estimates or failure of the voxel-SAIF algorithm to converge. Table 1 provides results of the bootstrap simulations. Mean values and s.d. of voxel-SAIF bootstrap estimates were in good agreement with parameter mean values and s.d. of the simulated reference values. *Bias%* and *RMSE%* of voxel-SAIF estimates for V_b, K_1, λ, and *rCPS* determined in 50 bootstrap simulations for three ROIs are also provided. *Bias* (<2%) and *RMSE* (<8%) were both low in estimates of λ. Estimates of *rCPS* had limited biases (3.9% to 6.0%) and variability consistent with the high level of noise typical of voxel-*TACs* (*RMSE* 17.3% to 19.7%). Blood volume, V_b, was also estimated with good accuracy ($\max_{Bias\%}$ 6.2%) but not high precision ($\max_{RMSE\%}$ 21.5%), particularly in corona radiata. Similar results were obtained for K_1 ($\max_{Bias\%}$ 9.2%; $\max_{RMSE\%}$ 12.7%).

Table 1 Performance of SAIF algorithm in bootstrap simulation[a]

Region[b]	V_b *(unitless)*	K_1 *(mL g^{-1} min^{-1})*	λ *(unitless)*	rCPS *(nmol g^{-1} min^{-1})*
Whole slice (11,081 voxels)				
Simulated reference values[c]	0.068 ± 0.050	0.048 ± 0.017	0.68 ± 0.14	1.68 ± 0.92
Voxel-SAIF estimates[d]	0.066 ± 0.049	0.051 ± 0.019	0.68 ± 0.14	1.73 ± 0.89
Voxel-SAIF Bias%[e]	0.1%	7.2%	0.9%	4.7%
Voxel-SAIF RMSE%[f]	17.2%	12.0%	7.4%	19.7%
Regional voxel-SAIF estimates[g]	0.066 ± 0.0001	0.051 ± 0.0001	0.68 ± 0.001	1.73 ± 0.003
ROI-SAIF estimates[h]	0.068 ± 0.0002	0.049 ± 0.0002	0.69 ± 0.002	1.54 ± 0.013
Frontal cortex (1,166 voxels)				
Simulated reference values[c]	0.076 ± 0.043	0.055 ± 0.023	0.67 ± 0.24	2.00 ± 1.00
Voxel-SAIF estimates[d]	0.074 ± 0.042	0.059 ± 0.025	0.67 ± 0.24	2.04 ± 1.00
Voxel-SAIF Bias%[e]	−2.4%	6.5%	0.9%	3.9%
Voxel-SAIF RMSE%[f]	12.5%	10.9%	7.1%	17.3%
Regional voxel-SAIF estimates[g]	0.074 ± 0.0002	0.059 ± 0.0002	0.67 ± 0.001	2.04 ± 0.007
ROI-SAIF estimates[h]	0.075 ± 0.0004	0.055 ± 0.0004	0.69 ± 0.004	1.78 ± 0.025
Corona radiata (1,837 voxels)				
Simulated reference values[c]	0.036 ± 0.020	0.030 ± 0.011	0.71 ± 0.25	0.91 ± 0.54
Voxel-SAIF estimates[d]	0.038 ± 0.022	0.033 ± 0.013	0.71 ± 0.25	0.96 ± 0.47
Voxel-SAIF Bias%[e]	6.2%	9.2%	1.6%	6.0%
Voxel-SAIF RMSE%[f]	21.5%	12.7%	6.4%	19.2%
Regional voxel-SAIF estimates[g]	0.038 ± 0.0003	0.033 ± 0.0001	0.71 ± 0.001	0.96 ± 0.005
ROI-SAIF estimates[h]	0.041 ± 0.0005	0.032 ± 0.0004	0.71 ± 0.008	0.94 ± 0.028

rCPS, regional rate of cerebral protein synthesis; *RMSE*, root mean square error; ROI, region of interest; SAIF, spectral analysis with iterative filter; V_b, fraction of volume occupied by blood.

[a]Number of bootstrap realizations = 50.

[b]Regions were limited to particular slice used for the bootstrap simulation.

[c]Values are mean ± intervoxel s.d. of the simulated voxel parameters within the region.

[d]Values are mean ± intervoxel s.d. of the estimated SAIF-voxel parameters from bootstrap simulations.

[e]Values are mean values of SAIF-voxel parameter *bias*% calculated over the bootstrap simulations.

[f]Values are mean values of SIAF-voxel parameter *RMSE*% calculated over the bootstrap simulations.

[g]Values are mean ± s.d. of the mean SAIF-voxel parameter estimates within the region, calculated over the bootstrap simulations.

[h]Values are mean ± s.d. of the ROI-SAIF parameter estimates calculated over the bootstrap simulations.

Normalizing and rescaling led to a small reduction (mean: 5%; range: 0% to 13%) in the standard deviation of the resampled residual values compared to those of the reference data set (see Supplementary Figure).

Table 1 also shows comparisons between voxel-SAIF estimates for the parameters, averaged over each ROI, and the corresponding parameters estimated with ROI-SAIF. Estimates of λ, V_b, and K_1 show good agreement between voxel and ROI methods. Regional rate of cerebral protein synthesis, which has a small positive bias ($\leqslant$6%) when estimated on a voxel-by-voxel basis, is underestimated with ROI-SAIF in the whole slice and frontal cortex by 8% and 11%, respectively. Variability of estimates of λ and *rCPS* among the 50 bootstrap simulations is lower for the mean of the voxel-SAIF estimates than those determined with ROI-SAIF.

Spectral Analysis with Iterative Filter Application to Measured Positron Emission Tomography Data

In measured PET data, the percentage of voxels in a given ROI in which voxel-SAIF either failed to converge or produced nonphysiological estimates, averaged over all subjects, ranged from 0.7% (Putamen) to 2.9% (Amygdala), depending on the brain area. The mean fraction of outlier voxels over all brain regions was 1.3%, and ~0.2% of voxels were excluded for failure to converge. The percentage of voxels included in the analysis was >95% for all subjects and regions. In whole brain 0.5% of voxels and in white matter 0.8% of voxels (mean over all subjects) had rates of protein synthesis not detectably different from zero. Figure 2 shows parametric maps for *rCPS*, λ, and K_1 in a representative transaxial slice at level of frontal cortex in one subject. The subject's MRI is also shown. In this slice, *rCPS* was 1.73 ± 0.96 nmol g^{-1} min^{-1} (mean ± s.d. over all brain voxels), 5th to 95th percentile range 0.04 to 3.01 nmol g^{-1} min^{-1}. Regional rate of cerebral protein synthesis shows the well-known pattern with areas of white matter tending to have lower *rCPS* than gray matter. Voxel-SAIF estimates of λ were 0.68 ± 0.11 (mean ± s.d.), corresponding to intraslice variability of ~16%. Although noisy, the λ image shows a tendency of higher values in white than gray matter areas. The 5th to 95th percentile range of K_1 estimates was 0.023 to 0.064 mL g^{-1} min^{-1}; there is a clear spatial distribution of higher and

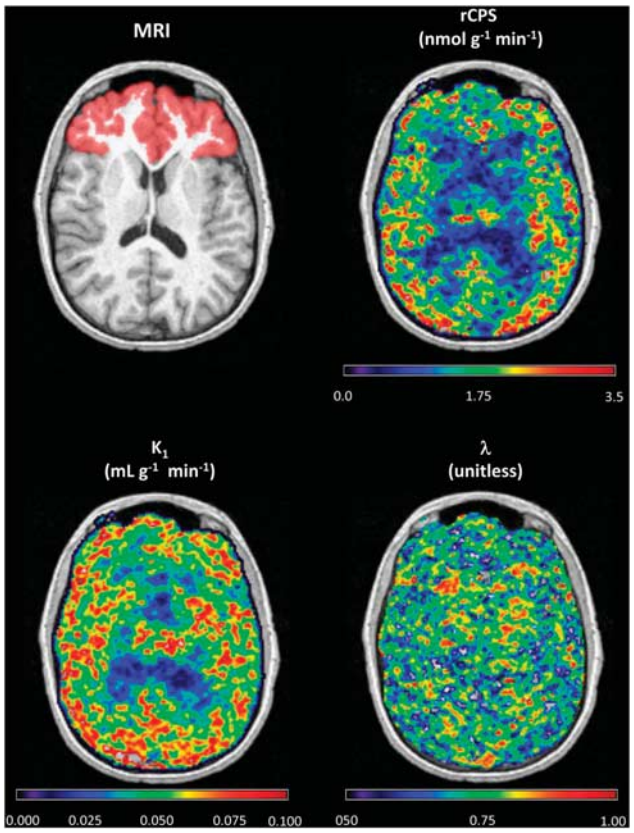

Figure 2 Magnetic resonance imaging (MRI) and parametric maps of regional rate of cerebral protein synthesis (*rCPS*), λ, and K_1 obtained with voxel-spectral analysis with iterative filter (SAIF). Images are of a representative transaxial slice for one subject. Red area in the MRI image represents the frontal cortex region for the particular slice. A Gaussian filter (full width at half maximum (FWHM) 1.7 mm) was employed to smooth each of the parametric images in three dimensions before visualization.

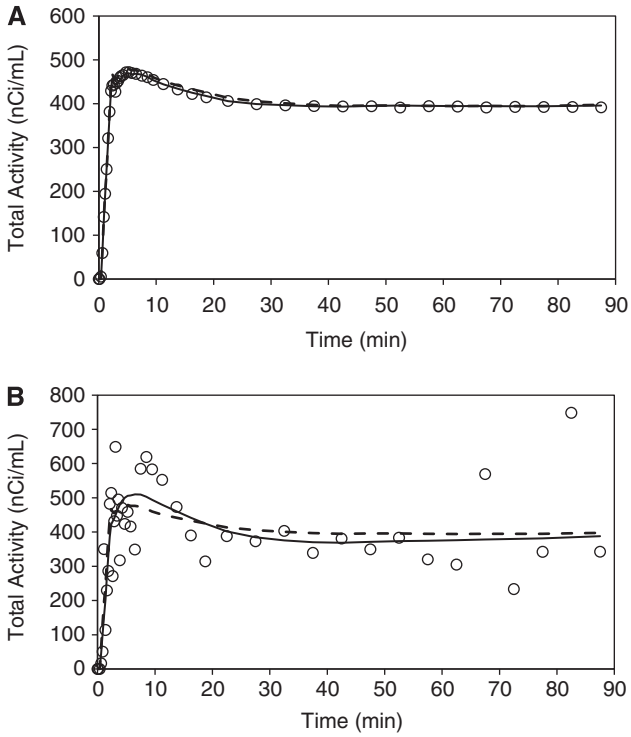

Figure 3 (**A**) Kinetic model fit of a region-of-interest (ROI) time-activity curve (*TAC*). Open circles (○) indicate activity measured in the whole brain region of one subject. Solid line represents activity estimated by fitting the ROI *TAC* with spectral analysis with iterative filter (SAIF). Dashed line represents mean of the fitted voxel-*TACs* within the ROI. (**B**) Kinetic model fit of a single voxel-*TAC* in the frontal cortex. Open circles (○) indicate activity measured in a single brain voxel. Solid line represents activity estimated by fitting the voxel-*TAC* with SAIF. Dashed line represents mean of the fitted voxel-*TACs* within the ROI.

lower values concentrated in gray and white matter, respectively.

Comparison of Voxel-Spectral Analysis with Iterative Filter and ROI-Spectral Analysis with Iterative Filter in Measured Positron Emission Tomography Data

Spectral analysis with iterative filter fits of ROI and voxel-*TACs* are shown in Figure 3. Overall, good agreement is seen when the mean of voxel-SAIF fits is compared with the ROI-SAIF fit of ROI *TAC* (Figure 3A). There are, however, small discrepancies: the mean voxel-SAIF fit slightly overestimates the measured activity between ~2 and 30 minutes, whereas the ROI-SAIF fit has a slight underestimation ~2 to 8 minutes and a very slight overestimation from ~15 to 25 minutes. After ~30 minutes, fits of the two methods are indistinguishable. The measured single voxel-*TAC* shown in Figure 3B illustrates the very high noise level present in voxel data and the variability between individually fit voxel-*TACs* (solid line) and the mean of all voxel-*TACs* in the region (dashed line).

Table 2 compares regional mean voxel-SAIF estimates with estimates determined with ROI-SAIF in measured PET data. Mean values and standard deviations for six subjects are reported for 12 ROIs and whole brain. There was excellent agreement between methods in estimates of V_b, K_1, and λ; mean relative differences were $1\% \pm 4\%$, $-1\% \pm 4\%$, and $-2\% \pm 2\%$ (mean ± s.d. among regions) for V_b, K_1, and λ, respectively (Table 2). Except in corona radiata, estimates of *rCPS* were somewhat higher with voxel-SAIF compared with ROI-SAIF; the mean percent difference between methods ranged from 2% (putamen) to 16% (occipital cortex), with average over all regions ~7.7%. Differences between voxel- and ROI-SAIF estimates of *rCPS* tended to be larger in cortical than in subcortical or white matter regions.

Figure 4 provides scatter plots that compare ROI-SAIF estimates of V_b, K_1, λ, and *rCPS* with voxel-SAIF estimates averaged over the same ROI. All ROIs and all subjects are included. In each plot, the

Table 2 Regional estimates of V_b, K_1, λ, and *rCPS*[a]

***Voxel-SAIF*[b]**

Region	*Region size (number of voxels)*	V_b	K_1 *(mL g^{-1} min^{-1})*	λ	rCPS *(nmol g^{-1} min^{-1})*
Whole brain	808,068 ± 88,180	0.073 ± 0.010	0.043 ± 0.007	0.73 ± 0.02	1.77 ± 0.07
Cerebellum	75,640 ± 6,080	0.094 ± 0.013	0.053 ± 0.009	0.72 ± 0.02	2.21 ± 0.10
Cortical					
Frontal cortex	85,452 ± 17,015	0.073 ± 0.013	0.047 ± 0.008	0.71 ± 0.03	2.02 ± 0.06
Temporal cortex	42,125 ± 6,437	0.075 ± 0.011	0.044 ± 0.007	0.71 ± 0.02	1.90 ± 0.09
Occipital cortex	26,971 ± 10,079	0.090 ± 0.017	0.055 ± 0.008	0.72 ± 0.03	2.30 ± 0.14
Parietal cortex	13,127 ± 3,241	0.079 ± 0.014	0.048 ± 0.007	0.71 ± 0.02	2.10 ± 0.14
Subcortical					
Thalamus	12,757 ± 1,862	0.073 ± 0.012	0.043 ± 0.008	0.74 ± 0.01	1.59 ± 0.10
Caudate	6,038 ± 784	0.050 ± 0.009	0.035 ± 0.007	0.76 ± 0.02	1.12 ± 0.11
Putamen	6,488 ± 794	0.061 ± 0.011	0.047 ± 0.010	0.78 ± 0.01	1.37 ± 0.06
Hippocampus	3,709 ± 1,080	0.088 ± 0.014	0.034 ± 0.006	0.69 ± 0.03	1.68 ± 0.19
Amygdala	3,522 ± 516	0.069 ± 0.012	0.031 ± 0.004	0.68 ± 0.03	1.60 ± 0.12
White matter					
Corona radiata	32,655 ± 3,350	0.035 ± 0.007	0.027 ± 0.005	0.76 ± 0.03	0.90 ± 0.06
Cerebellar peduncles	9,554 ± 1,227	0.054 ± 0.010	0.036 ± 0.007	0.75 ± 0.02	1.25 ± 0.10

***ROI-SAIF*[c]**

Region	V_b	K_1 *(mL g^{-1} min^{-1})*	λ	rCPS *(nmol g^{-1} min^{-1})*
Whole brain	0.074 ± 0.011	0.045 ± 0.007	0.75 ± 0.03	1.58 ± 0.10
Cerebellum	0.095 ± 0.012	0.056 ± 0.010	0.75 ± 0.02	2.00 ± 0.18
Cortical				
Frontal cortex	0.070 ± 0.013	0.048 ± 0.009	0.74 ± 0.03	1.76 ± 0.05
Temporal cortex	0.076 ± 0.012	0.043 ± 0.007	0.72 ± 0.02	1.75 ± 0.12
Occipital cortex	0.085 ± 0.016	0.057 ± 0.008	0.75 ± 0.03	1.99 ± 0.12
Parietal cortex	0.074 ± 0.014	0.050 ± 0.007	0.74 ± 0.03	1.87 ± 0.25
Subcortical				
Thalamus	0.070 ± 0.012	0.044 ± 0.008	0.77 ± 0.02	1.39 ± 0.05
Caudate	0.051 ± 0.009	0.033 ± 0.007	0.77 ± 0.03	1.07 ± 0.07
Putamen	0.059 ± 0.011	0.046 ± 0.008	0.78 ± 0.02	1.34 ± 0.07
Hippocampus	0.089 ± 0.014	0.032 ± 0.006	0.68 ± 0.03	1.59 ± 0.24
Amygdala	0.073 ± 0.012	0.030 ± 0.004	0.68 ± 0.04	1.51 ± 0.12
White matter				
Corona radiata	0.037 ± 0.007	0.027 ± 0.006	0.75 ± 0.03	0.93 ± 0.06
Cerebellar peduncles	0.052 ± 0.009	0.039 ± 0.007	0.78 ± 0.03	1.16 ± 0.18

***Mean relative difference*[d] *and correlation*[e]**

Region	V_b		K_1		λ		rCPS	
	mrd	R^2	mrd	R^2	mrd	R^2	mrd	R^2
Whole brain	0%	0.99	−4%	0.99	−3%	0.81	12%	0.51
Cerebellum	−1%	0.99	−5%	1.00	−4%	0.89	10%	0.81
Cortical								
Frontal cortex	4%	0.99	−1%	1.00	−4%	0.88	15%	0.73
Temporal cortex	−1%	0.99	1%	0.99	−2%	0.68	9%	0.54
Occipital cortex	5%	1.00	−4%	0.99	−5%	0.97	16%	0.76
Parietal cortex	6%	0.99	−4%	0.99	−4%	0.60	12%	0.76
Subcortical								
Thalamus	4%	1.00	−4%	0.99	−4%	0.85	14%	0.58
Caudate	−1%	0.96	5%	0.98	0%	0.50	5%	0.79
Putamen	3%	0.99	2%	0.99	0%	0.62	2%	0.89
Hippocampus	−2%	0.99	6%	0.99	2%	0.65	6%	0.90
Amygdala	−5%	0.99	4%	0.92	1%	0.56	6%	0.82
White matter								
Corona radiata	−6%	0.98	0%	0.98	1%	0.89	−2%	0.56
Cerebellar peduncles	4%	0.98	−9%	0.99	−4%	0.87	8%	0.85

rCPS, regional rate of cerebral protein synthesis; ROI, region of interest; SAIF, spectral analysis with iterative filter; *TAC*, time-activity curve; V_b, fraction of volume occupied by blood.

[a]Values are mean ± s.d. for six subjects.

[b]Voxel-SAIF estimates based on voxel *TACs* and optimal voxel-SAIF filter; weights based on the whole brain *TAC*; parameters averaged over the volume of interest.

[c]ROI-SAIF estimates based on the ROI *TACs* and optimal ROI-SAIF filter; weights based on the ROI *TAC*.

[d]For each region, mean relative difference (*mrd*) based on the percent relative difference between voxel-SAIF and ROI-SAIF estimates, averaged among subjects.

[e]Regional estimate correlation, between voxel-SAIF and ROI-SAIF, indicated by Pearsons's coefficient (R^2).

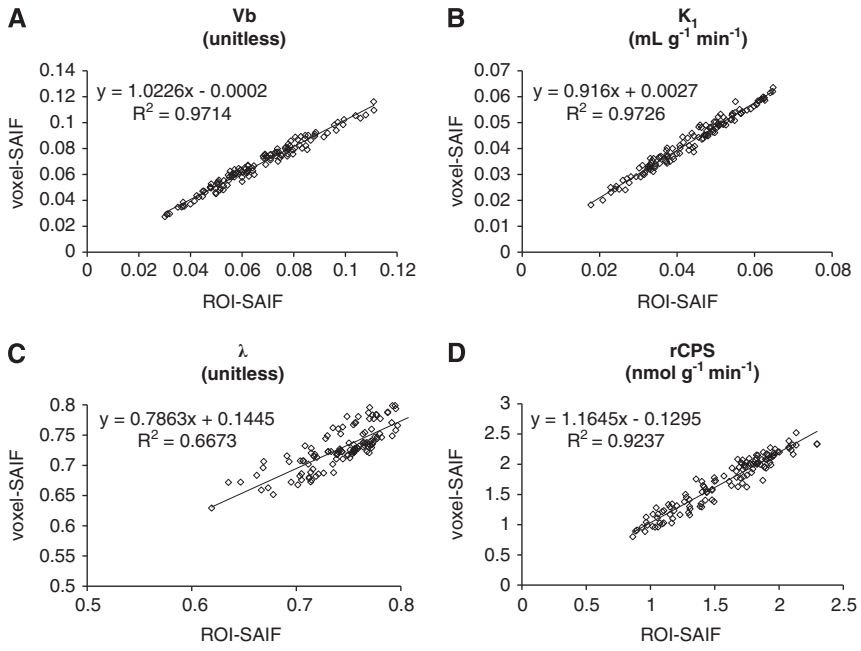

Figure 4 Scatter plots of regional rate of cerebral protein synthesis (*rCPS*) (**A**), λ (**B**), K_1 (**C**), and V_b (**D**). Parameter values estimated using region-of-interest spectral analysis with iterative filter (ROI-SAIF) are plotted on the *x* axis and the average (over all voxels in the ROI) of the parameters estimated using voxel-SAIF are on the *y* axis. All subjects and ROIs are included. In each scatter plot, the slope and intercept of the fitted regression line and Pearson's R^2 are reported.

equation of the estimated regression line and Pearson's correlation coefficient are reported. V_b, K_1, and *rCPS* show close correlation between voxel-SAIF and ROI-SAIF estimates ($R^2 > 0.92$). Estimates of λ are less tightly correlated ($R^2 = 0.67$).

Heterogeneity Analysis

From analysis of the simulated reference and bootstrap-estimated number of equilibrating components, we evaluated the capacity of voxel-SAIF to correctly determine the number of compartments in the tissue voxel. In 72.3% of voxels, the number of equilibrating components estimated with voxel-SAIF agreed with simulated reference values. In the remaining 27.7%, voxel-SAIF detected a lower (11.4%) or higher (16.3%) number of equilibrating components compared with the reference number. A trapping component was correctly detected in 100% of simulated voxel-*TACs*.

This behavior is similar to ROI-SAIF performance in simulation, where the accuracy rate for correct determination of number of equilibrating components was 73.1%. In the ROI data, however, ROI-SAIF detected a higher number of equilibrating components in 26% of cases and a lower number in only 1% of regions. As in the voxelwise analysis, a trapping component was correctly detected in all simulated ROIs.

In measured data, differences in the number of detected tissue components were found between the voxelwise and ROI-level analyses, as might be expected. In ROI-SAIF one trapping component, one blood component, and at least two equilibrating components were detected in all regions and subjects. With voxel-SAIF, one trapping and one blood component were found in 100% of successfully estimated voxels, but only 45% of them included two or more equilibrating components. The finding of more than one equilibrating component suggests kinetic heterogeneity of the tissue in these voxels. In the remaining voxels, only one equilibrating component was detected, indicating the homogenous tissue model was appropriate to describe 55% of brain voxel-*TACs*.

Figure 5 illustrates the spatial distribution of voxels in which two equilibrating components were detected in a representative transaxial slice at the cortical level. From the distribution it appears that the concentration of kinetically inhomogenous voxels is higher at the border between gray and white matter than within the gray or white matter itself. A similar pattern was found in all subjects and brain slices.

Discussion

Before this study, voxelwise estimation of kinetic model parameters of L-[1-^{11}C]leucine could only be performed by a method that assumes kinetic homogeneity of tissue within the voxel (Tomasi *et al*, 2009). Observed differences between measured and

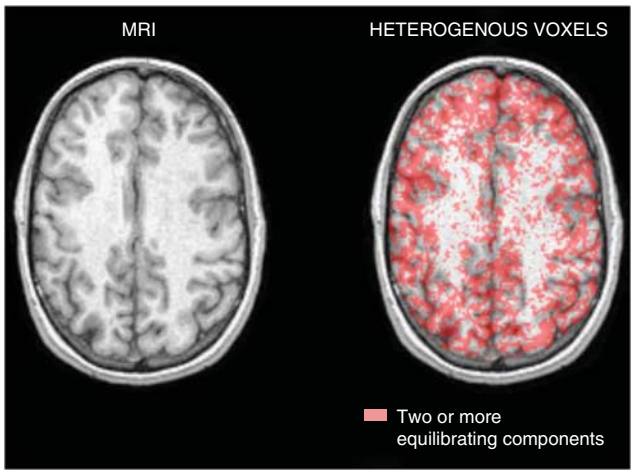

Figure 5 Magnetic resonance imaging (MRI) and spatial distribution of heterogeneous voxels. T1-weighted MR image (left) and the same image fused with the spatial distribution of voxels estimated to be heterogeneous (right). The red area corresponds to those voxels in which voxel-spectral analysis with iterative filter (SAIF) detects two or more equilibrating components.

fitted *TACs* suggested that effects of tissue heterogeneity had not been entirely eliminated by performing analyses at the voxel rather than the ROI level (Tomasi *et al*, 2009). The SAIF method (Veronese *et al*, 2010*a*) was developed to specifically allow for tissue heterogeneity in the kinetic model for leucine used for *rCPS* quantification. In the present study, we explored use of SAIF for quantification of *rCPS* from L-[1-^{11}C]leucine data at the voxel level to understand the possible presence of kinetic heterogeneity at the voxel level and its impact on *rCPS* estimates.

Setting the passband filter limits and assessing performance of SAIF at the voxel level was carried out in two simulations that used different noise generation methods. To be consistent with the strategy defined in Veronese *et al* (2010*a*) for selection of the passband, we used a Monte Carlo approach, a standard method for noise generation in simulation, widely used and easy to implement. Due to the high noise levels, however, the Monte Carlo approach led to simulated *TACs* in some voxels with negative activity values. To avoid negative activities in simulated *TACs*, we utilized bootstrapping of residuals for noise generation in the simulation to assess performance of voxel-SAIF. Negative entries in simulated *TACs* were avoided by normalizing reference residuals and rescaling the resampled residuals by the maxima of the associated *TACs*; this choice of scale factors had only a modest effect on noise variance. Results of the two types of simulation were consistent: performance indices for *rCPS* and other parameters were comparable. Of note, in addition to the assumption of equal residual variances discussed previously, the bootstrap approach assumes that residuals have zero-mean and are statistically independent. The zero-mean assumption was easy to verify (mean of voxel residuals: −0.002 nCi/mL). The statistical independence assumption is known to be incompletely met for voxel data: the process of PET data reconstruction leads to spatial correlation between nearby voxels, although correlation drops off rapidly as distance between voxels increases (Pajevic *et al*, 1998). Accounting for spatial correlation is a difficult statistical problem beyond the scope of the present study. Methods that perform kinetic modeling in a transformed space, for example, in the wavelet domain, can account for spatial correlation in the data, but apply only to models in which the estimation operator is linear in the data, such as a Patlak plot or Logan analysis (Turkheimer *et al*, 2000). Further investigation is needed to determine the performance of these methods with voxel-SAIF analysis. We utilized here the routinely used approach that treats each voxel-*TAC* as independent from the others.

One remarkable outcome of the analysis was the good performance of voxel-SAIF in estimation of leucine kinetic parameters and *rCPS*. When simulated reference values were compared with bootstrap-estimated parameters, voxel-SAIF demonstrated low bias and good precision. Moreover, voxel-SAIF produced a low number of outliers. Essential to the performance of voxel-SAIF was selection of an appropriate passband whose role is to reduce the influence of noise on parameter estimates. The optimal voxel-SAIF passband filter differed somewhat from that used for ROI-SAIF. In particular, high-frequency noise present in voxel data but attenuated in the ROI data reduces the accuracy with which high-frequency components can be estimated. The upper bound for the voxel-SAIF passband filter was more selective compared to the filter for ROI-SAIF (0.2 min^{-1} instead of 0.3 min^{-1}); this reduces the impact of high-frequency noise. At the other end of the spectrum, the less restrictive lower bound of the voxel-SAIF passband (0.02 min^{-1} for voxel-SAIF; 0.03 min^{-1} for ROI-SAIF) has the effect of allowing greater kinetic variability in low-frequency components among individual brain voxels.

In measured data, when means of voxel-SAIF estimates within a region were compared with ROI-SAIF estimates, there was generally good agreement between analysis methods. Unlike fixed compartmental model analyses, spectral analysis allows the tissue ROI to be represented as a linear combination of any number of tissue compartments. Because the tissue ROI could be represented as a linear combination of the compartments of each voxel comprising the ROI, we could expect good agreement between the ROI-SAIF estimates and mean voxel-SAIF estimates of linear parameters of the model. Indeed, the linear parameter V_b and the parameter K_1, which is the sum of the linear coefficients α_i, exhibit the best agreement (1% ± 4% and 1% ± 4%, mean ± s.d. of the difference between ROI-SAIF and mean voxel-SAIF estimates of V_b and

K_1, respectively) and highest correlation between methods (0.97 for both V_b and K_1).

In contrast to linear parameters, λ and *rCPS* are nonlinear combinations of parameters, and therefore less agreement between ROI-SAIF and mean voxel-SAIF estimates is to be expected. Estimates of λ were $2\% \pm 2\%$ higher with ROI-SAIF and correlation between estimates provided by the two methods was 0.67. Correlation between *rCPS* estimated with the two methods was very high ($R^2 = 0.92$), but estimates were $8\% \pm 6\%$ lower with ROI-SAIF. Determination of λ from the SAIF-estimated coefficients α_i is based on the assumption that all λ in the subregions of a heterogeneous tissue are equal; this constraint is likely to have a greater impact when data are analyzed at the ROI level, where a uniform value of λ for the entire region is assumed, than when data are analyzed at the voxel level and λ can vary among voxels within the region. The constraint contributes to differences between ROI-SAIF and voxel-SAIF estimates of λ and, by extension (equation), estimates of *rCPS*.

Spectral analysis can also be used to provide information on number of compartments in the kinetic model of the tracer in tissue. For the tracer L-[1-^{11}C]leucine, each equilibrating compartment corresponds to the precursor pool of L-[1-^{11}C]leucine in a kinetically homogeneous tissue that exchanges with the plasma. Multiple exchangeable compartments suggest that the tissue is kinetically heterogeneous. When applied to measured PET data, voxel-SAIF found multiple equilibrating tissue compartments in $\sim$45% of the brain voxels. In the remaining voxels one equilibrating compartment, that is, a homogeneous tissue model, was found to adequately describe the data. Spectral analysis with iterative filter accuracy in determining the correct number of compartments was $>70\%$; in the remaining voxels SAIF had a tendency to overestimate the number of tissue equilibrating components, at the ROI as well as at the voxel level. This is typical of spectral analysis methods—since they are not constrained by a fixed model, they tend to add extra components into the model in order to provide a better fit of the data, and this behavior is particularly evident at high noise levels. The inclusion of extra compartments, however, does not have a significant impact on voxel-SAIF estimates, as evidenced by the good performance statistics found in the bootstrap simulation data.

Analysis of the spatial maps of heterogeneous voxels, in which voxel-SAIF selected the heterogeneous kinetic model to describe the voxel-*TACs*, suggests the presence of a distribution pattern: in our scans heterogeneous voxels appear to be concentrated at the borders between gray and white matter. This finding was somewhat surprising; we had expected more gray matter voxels to be considered heterogeneous due to inherent gray matter heterogeneity, for example, differences in *rCPS* among the cortical layers, and partial volume effects arising from the limited spatial resolution of the scanner. The partial volume effects would be greater, and therefore more voxels may be considered as heterogeneous, in lower-resolution scans. The present results do, however, confirm that use of a homogenous kinetic model to describe voxel-*TACs* is not appropriate for all voxels in brain, even on a high-resolution scanner.

Use of the iterative filter implemented in SAIF improved the robustness of the method to noise; voxel-SAIF provided good estimates of leucine kinetic parameters and *rCPS*, even at high noise levels. Region-of-interest-based- and mean voxel-based-*rCPS* estimates were highly correlated, but ROI-based estimates were higher. Simulations showed that mean voxel-level *rCPS* estimates had lower bias than ROI-based estimates in whole brain and cortex, had comparable bias in white matter, and had lower variability in all regions. We conclude that estimation of *rCPS* with SAIF is improved when the method is applied at the voxel level. Voxel-SAIF may also provide useful information about the spatial distribution of voxel heterogeneity.

Disclosure/conflict of interest

The authors declare no conflict of interest.

References

Bertoldo A, Vicini P, Sambuceti G, Lammertsma AA, Parodi O, Cobelli C (1998) Evaluation of compartmental and spectral analysis models of [^{18}F]FDG kinetics for heart and brain studies with PET. *IEEE Trans Biomed Eng* 45:1429–48

Bishu S, Schmidt KC, Burlin T, Channing M, Conant S, Huang T, Liu Z-H, Qin M, Vuong B, Unterman A, Xia Z, Zametkin A, Herscovitch P, Smith CB (2008) Regional rates of cerebral protein synthesis measured with L-[1-^{11}C]leucine and PET in conscious, young adult men: normal values, variability, and reproducibility. *J Cereb Blood Flow Metab* 28:1502–13

Bishu S, Schmidt KC, Burlin T, Channing M, Horowitz L, Huang T, Liu Z-H, Qin M, Vuong B, Unterman A, Xia Z, Zametkin A, Herscovitch P, Quezado Z, Smith CB (2009) Propofol anaesthesia does not alter regional rates of cerebral protein synthesis measured with L-[1-^{11}C]leucine and PET in healthy male subjects. *J Cereb Blood Flow Metab* 29:1035–47

Brooks DJ, Lammertsma AA, Beaney RP, Leenders KL, Buckingham PD, Marshall J, Jones T (1984) Measurement of regional cerebral pH in human subjects using continuous inhalation of $^{11}CO_2$ and positron emission tomography. *J Cereb Blood Flow Metab* 4:458–65

Buxton RB, Alpert NM, Babikian V, Weise S, Correia JA, Ackerman RH (1987) Evaluation of the $^{11}CO_2$ positron emission tomographic method for measuring brain pH. I. pH changes measured in states of altered PCO_2. *J Cereb Blood Flow Metab* 7:709–19

Carson R, Barker W, Liow J-S, Johnson C (2003) Design of a motion-compensation OSEM list-mode algorithm for resolution-recovery reconstruction for the HRRT. *IEEE Trans Nucl Sci* 5:3281–5

Cunningham VJ, Jones T (1993) Spectral analysis of dynamic PET studies. *J Cereb Blood Flow Metab* 13:15–23

Efron B (1979) Bootstrap methods: another look at the jackknife. *Ann Statist* 7:1–26

Lajtha A, Latzkovits L, Toth J (1976) Comparison of turnover rates of proteins of the brain, liver and kidney in mouse *in vivo* following long term labeling. *Biochim Biophys Acta* 425:511–20

Pajevic S, Daube-Witherspoon ME, Bacharach SL, Carson RE (1998) Noise characteristics of 3-D and 2-D PET images. *IEEE Trans Med Imag* 17:9–23

Siesjo BK, Thompson WO (1965) The rate of incorporation of gaseous $^{14}CO_2$ into brain tissue constituents. *Experientia* 20:98–9

Schmidt KC (1999) Which linear compartmental systems can be analyzed by spectral analysis of PET output data summed over all compartments? *J Cereb Blood Flow Metab* 19:560–9

Schmidt KC, Cook MP, Qin M, Kang J, Burlin TV, Smith CB (2005) Measurement of regional rates of cerebral protein synthesis with L-[1-^{11}C]leucine and PET with correction for recycling of tissue amino acids: I. Kinetic modeling approach. *J Cereb Blood Flow Metab* 25:617–28

Schmidt KC, Smith CB (2005) Resolution, sensitivity and precision with autoradiography and small animal positron emission tomography: implications for functional brain imaging in animal research. *Nucl Med Biol* 32:719–25

Schmidt KC, Turkheimer FE (2002) Kinetic modeling in positron emission tomography. *Q J Nucl Med* 46:70–85

Smith CB, Schmidt KC, Qin M, Burlin TV, Cook MP, Kang J, Saunders RC, Bacher JD, Carson RE, Channing MA, Eckelman WC, Herscovitch P, Laverman P, Vuong BK (2005) Measurement of regional rates of cerebral protein synthesis with L-[1-^{11}C]leucine and PET with correction for recycling of tissue amino acids: II. Validation in rhesus monkeys. *J Cereb Blood Flow Metab* 25:629–40

Tomasi G, Bertoldo A, Bishu S, Unterman A, Smith CB, Schmidt K (2009) Voxel-based estimation of kinetic model parameters of the L-[1-^{11}C]leucine PET method for determination of regional rates of cerebral protein synthesis: validation and comparison with region-of-interest-based methods. *J Cereb Blood Flow Metab* 29:1317–31

Turkheimer F, Moresco RM, Lucignani G, Sokoloff L, Fazio F, Schmidt K (1994) The use of spectral analysis to determine regional cerebral glucose utilization with positron emission tomography and [18F]fluorodeoxyglucose: theory, implementation, and optimization procedures. *J Cereb Blood Flow Metab* 14: 406–422

Turkheimer FE, Banati RB, Visvikis D, Aston JAD, Gunn RN, Cunningham VJ (2000) Modeling dynamic PET-SPECT studies in the wavelet domain. *J Cereb Blood Flow Metab* 20:879–93

Veronese M, Bertoldo A, Bishu S, Unterman A, Tomasi G, Smith CB, Schmidt KC (2010*a*) A spectral analysis approach for determination of regional rates of cerebral protein synthesis with the L-[1-(11)C]leucine PET method. *J Cereb Blood Flow Metab* 30:1460–76

Veronese M, Bertoldo A, Schmidt KC (2010*b*) A spectral analysis approach for voxelwise determination of regional rates of cerebral protein synthesis with the L-[1-(11)C]leucine PET method, Neuroimage, Volume 52, Supplement 1, Eighth International Symposium on Functional Neuroreceptor Mapping of the Living Brain, 22–24 June 2010, Glasgow, UK

Wienhard K, Schmand M, Casey ME, Baker K, Bao J, Eriksson L, Jones WF, Knoess C, Lenox M, Lercher M, Luk P, Michel C, Reed JH, Richerzhagen N, Treffert J, Vollmar S, Young JW, Heiss WD, Nutt R (2002) The ECAT HRRT: performance and first clinical application of the new high resolution research tomograph. *IEEE Trans Nucl Sci* 49:104–10

Wu Y, Carson R (2002) Noise reduction in the simplified reference tissue model for neuroreceptor functional imaging. *J Cereb Blood Flow Metab* 22:1440–52

Supplementary Information accompanies the paper on the Journal of Cerebral Blood Flow & Metabolism website (http://www.nature.com/jcbfm)